REPORT DOCUMENTATION PAGE

Public reporting burden for this collection of information is estimated to average 1 hour per response, including the time for reviewing instructions, searching data sources, gathering and maintaining the data needed, and completing and reviewing the collection of information. Send comments regarding this burden estimate or any other aspect of this collection of information, including suggestions for reducing this burden to Washington Headquarters Service, Directorate for Information Operations and Reports, 1215 Jefferson Davis Highway, Suite 1204, Arlington, VA 22202-4302, and to the Office of Management and Budget, Paperwork Reduction Project (0704-0188) Washington, DC 20503.
PLEASE DO NOT RETURN YOUR FORM TO THE ABOVE ADDRESS.

1. REPORT DATE *(DD-MM-YYYY)*	2. REPORT DATE	3. DATES COVERED *(From - To)*
22-11-2002	Technical	0101-1992 to 31-12-2003

4. TITLE AND SUBTITLE

Generalized-a time integration solutions for hanging chain dynamics

5a. CONTRACT NUMBER

5b. GRANT NUMBER

N00014-92-J-1269

5c. PROGRAM ELEMENT NUMBER

6. AUTHOR(S)

Jason I. Gobat
Mark A. Grosenbaugh
Michael S. Triantofyllou

5d. PROJECT NUMBER

5e. TASK NUMBER

5f. WORK UNIT NUMBER

7. PERFORMING ORGANIZATION NAME(S) AND ADDRESS(ES)

Woods Hole Oceanographic Insitution
Woods Hole, MA 02543

8. PERFORMING ORGANIZATION REPORT NUMBER

9. SPONSORING/MONITORING AGENCY NAME(S) AND ADDRESS(ES)

Office of Naval Research
Environemntal Sciences Directorate
Arlington, VA 22217-5660

10. SPONSOR/MONITOR'S ACRONYM(S)

11. SPONSORING/MONITORING AGENCY REPORT NUMBER

12. DISTRIBUTION AVAILABILITY STATEMENT

APPROVED FOR PUBLIC RELEASE - DISTRIBUTION IS UNLIMITED

13. SUPPLEMENTARY NOTES

In citiing the report in abibliography, the reference given should read: Journal of Engineering Mechanics, 128(6):677-687

14. ABSTRACT

Abstract: In this paper, we study numerically the two- and three-dimensional nonlinear dynamic response of a chain hanging under its own weight. Previous authors have employed the box method, a finite-difference scheme popular in cable dynamics problems, for this purpose. The box method has significant stability problems, however, and thus is not well suited to this highly nonlinear problem. We illustrate these stability problems and propose a new time integration procedure based on the generalized-α method. The new method exhibits superior stability properties compared to the box method and other algorithms such as backward differences and trapezoidal rule. Of four time integration methods tested, the generalized-α algorithm was the only method that produced a stable solution for the three-dimensional whirling motions of a hanging chain driven by harmonic linear horizontal motion at the top.

15. SUBJECT TERMS

nonlinear responses, finite differences, cables, numerical models, dynamics

16. SECURITY CLASSIFICATION OF:			17. LIMITATION OF ABSTRACT	18. NUMBER OF PAGES	19a. NAME OF RESPONSIBLE PERSON
a. REPORT	b. ABSTRACT	c. THIS PAGE			Mark Grosenbaugh
UL	UL	UL	UL	11	19b. TELEPONE NUMBER *(Include area code)* 508.289.2607

Standard Form 298 (Rev. 8-98)
Prescribed by ANSI-Std Z39-18

20021212 029

Generalized-α Time Integration Solutions for Hanging Chain Dynamics

Jason I. Gobat[1]; Mark A. Grosenbaugh[2]; and Michael S. Triantafyllou[3]

Abstract: In this paper, we study numerically the two- and three-dimensional nonlinear dynamic response of a chain hanging under its own weight. Previous authors have employed the box method, a finite-difference scheme popular in cable dynamics problems, for this purpose. The box method has significant stability problems, however, and thus is not well suited to this highly nonlinear problem. We illustrate these stability problems and propose a new time integration procedure based on the generalized-α method. The new method exhibits superior stability properties compared to the box method and other algorithms such as backward differences and trapezoidal rule. Of four time integration methods tested, the generalized-α algorithm was the only method that produced a stable solution for the three-dimensional whirling motions of a hanging chain driven by harmonic linear horizontal motion at the top.

Introduction

The dynamics of a chain hanging under its own weight is a classic problem in mechanics. Two of the more interesting aspects of the problem are the simultaneous presence of both high- and low-tension regimes in the chain and the unstable nature of large amplitude motions. Triantafyllou and Howell (1993) and Howell and Triantafyllou (1993) considered both of these phenomena using a combination of analytic, numerical, and experimental results. They observed that the stability of the response in a harmonically driven system is strongly dependent on the frequency and amplitude of the excitation.

The numerical model that they employed was based on a finite-difference scheme known as the box method. This method was first applied to a cable dynamics problem by Ablow and Schechter (1983). Because the box method is an implicit scheme, box method solutions for the classical cable dynamics equations are singular when the tension goes to zero anywhere on the cable. Howell and Triantafyllou (1993) removed this singularity by adding bending stiffness to the governing equations, thus providing a mechanism to propagate energy in the presence of zero tension (Burgess 1993). For small values of artificial bending stiffness

[1]Postdoctoral Invest., Dept. of Physical Oceanography, Woods Hole Oceanographic Institution, Mail Stop No. 29, Woods Hole, MA 02543. E-mail: jgobat@whoi.edu

[2]Associate Scientist, Dept. of Applied Ocean Physics and Engineering, Woods Hole Oceanographic Institution, Mail Stop No. 7, Woods Hole, MA 02543. E-mail: mgrosenbaugh@whoi.edu

[3]Professor, Dept. of Ocean Engineering, Massachusetts Institute of Technology, 77 Massachusetts Ave., Cambridge, MA 02139. E-mail: mistetri@deslab.mit.edu FAX 617-258-9389.

this modification stabilized the numerical solution with no loss of accuracy compared to experimental results.

The box method is popular because it is second-order accurate in both space and time and is relatively easy to implement. Because the box method preserves the frequency content of the solution across all frequencies, however, it has the disadvantage of relatively poor stability in its temporal discretization. In a nonlinear problem, spurious high-frequency content can cause numerical instabilities, and thus, it is desirous that a temporal integration scheme should be numerically dissipative at high frequencies. Koh et al. (1999) addressed this shortcoming of the box method by replacing the box method's temporal integration scheme with backward differences. They preserved the box method's straightforward and easy to implement spatial discretization. Backward differences have also been used by Chatjigeorgiou and Mavrakos (1999) and Chiou and Leonard (1991) in conjunction with spatial discretizations based on collocation and direct integration, respectively. The scheme is only first-order accurate, but is very stable because it has strong numerical dissipation at high frequencies.

Another temporal integration scheme that has been used in cable dynamics applications is the generalized trapezoidal rule (Sun et al. 1994). This scheme offers controllable numerical dissipation, but is second-order accurate only in its least dissipative form. Thomas (1993) compared three historically popular algorithms from the structural dynamics community, Newmark, Houbolt, and Wilson-θ, for use in mooring dynamics problems. His conclusion was that Houbolt was the best choice of the three. Other authors, however, have noted that Houbolt has an undesirable amount of low-frequency dissipation (Chung and Hulbert 1994; Hughes 1987).

Turning to the more recent structural dynamics literature, Gobat and Grosenbaugh (2001) proposed replacing the box method's temporal integration with the generalized-α method developed for the second-order structural dynamics problem by Chung and Hulbert (1993). This algorithm has the advantages of controllable numerical dissipation, second-order accuracy, and straightforward adaptation to the first-order nonlinear cable dynamics problem. Through appropriate choices of parameters, the method can also reproduce the spectral properties of several other algo-

rithms including the box method, backward differences, and trapezoidal rule. This latter property makes it a particularly convenient choice for the type of comparative study undertaken herein.

The analyses of the box and generalized-α methods from Gobat and Grosenbaugh (2001) are summarized below. The performance of the new algorithm is studied by comparison to analytic and experimental results for the free and forced response of the hanging chain. Throughout the analyses, comparisons are also made to trapezoidal rule and backward difference solutions.

Analysis of Box Method

The governing equations for a cable or chain can be written as a system of partial differential equations of the form (Howell 1992)

$$\mathbf{M}\frac{\partial \mathbf{Y}}{\partial t}+\mathbf{K}\frac{\partial Y}{\partial s}+\mathbf{F}(\mathbf{Y},s,t)=0 \qquad (1)$$

where $\mathbf{Y}=$ vector of N-dependent variables, $\mathbf{M}$ and $\mathbf{K}$ = coefficient matrices, and $\mathbf{F}=$ force vector. The independent variables are s, the Lagrangian coordinate measuring length along the unstretched cable, and t, time. Howell and Triantafyllou (1993) used the box method to discretize Eq. (1). In the box method the discrete equations are written using what look like traditional backward differences in both space and time, but because the discretization is applied on the half-grid points with spatial and temporal averaging of adjacent grid points, the method is second-order accurate. The result is a four-point average centered around the half-grid point.

The stability of the box method can be analyzed by considering an equivalent linear, single degree-of-freedom system in semidiscrete form. This approach separates the spatial and temporal discretizations into distinct procedures. For each of the $n-1$ spatial half-grid points between the n nodes a set of N discrete equations is assembled. Combining these $N(n-1)$ equations with N equations describing the boundary conditions yields the semidiscrete equation of motion for all of the dependent variables at all of the nodes as (Gobat and Grosenbaugh 2001)

$$\tilde{\mathbf{M}}\dot{\mathbf{Y}}+\tilde{\mathbf{K}}\mathbf{Y}+\tilde{\mathbf{F}}=0 \qquad (2)$$

The tilde over the matrices signifies that these are now discretized, assembled quantities. The single degree-of-freedom, linear, homogeneous analog of Eq. (2) is

$$\dot{y}+\omega y=0 \qquad (3)$$

Applying the box method's temporal discretization to Eq. (3) yields

$$\dot{y}^{i}+\dot{y}^{i-1}+\omega(y^{i}+y^{i-1})=0 \qquad (4)$$

where

$$\dot{y}^{i}+\dot{y}^{i-1}=2\left(\frac{y^{i}-y^{i-1}}{\Delta t}\right) \qquad (5)$$

Rearranging Eq. (5) gives the recursion relationships

$$\dot{y}^{i}=2\left(\frac{y^{i}-y^{i-1}}{\Delta t}\right)-\dot{y}^{i-1} \qquad (6)$$

$$y^{i}=\frac{\Delta t}{2}(\dot{y}^{i}+\dot{y}^{i-1})+y^{i-1} \qquad (7)$$

Substituting each of the recursion relationships separately into Eq. (4), we can write equations for y^{i} and $\dot{y}^{i}$ in matrix form as

$$\begin{bmatrix} y^{i} \\ \dot{y}^{i} \end{bmatrix}=\begin{bmatrix} \dfrac{2-\omega\Delta t}{2+\omega\Delta t} & 0 \\ \dfrac{-4}{2+\omega\Delta t} & -1 \end{bmatrix}\begin{bmatrix} y^{i-1} \\ \dot{y}^{i-1} \end{bmatrix} \qquad (8)$$

The 2×2 matrix on the right-hand side of Eq. (8) is the amplification matrix. Spectral radius ρ of this matrix, defined as

$$\rho=\max(|\lambda_{1}|,|\lambda_{2}|) \qquad (9)$$

governs the growth or decay of the solution from one time step to the next (Hughes 1987). $\lambda_{1,2}=$ eigenvalues of the amplification matrix. For $\rho\leq1$, the solution will remain steady or decay and is said to be stable. For $\rho>1$, the solution will grow and is said to be unstable. For the box method,

$$\lambda_{1}=\frac{2-\omega\Delta t}{2+\omega\Delta t} \qquad (10)$$

$$\lambda_{2}=-1 \qquad (11)$$

and the spectral radius is unity (and the scheme is stable) for all values of ω and Δt.

In spite of this unconditional stability, however, the box method has three significant problems. The first problem is illustrated by considering the update equation for y^{i} written in the form

$$y^{i}=\left(\frac{2-\omega\Delta t}{2+\omega\Delta t}\right)y^{i-1} \qquad (12)$$

As $\omega\Delta t$ goes to infinity this becomes

$$y^{i}=-y^{i-1} \qquad (13)$$

This is the phenomenon known as Crank–Nicholson noise, whereby the high-frequency components of the solution oscillate with every time step. A second, related, problem is that the spectral radius is constant at unity. An artifact of the spatial discretization process is that at some point the high-frequency (or equivalently, high-spatial wave-number) components of the solution are not well resolved and the numerical solution is inaccurate. For this reason it is desirous to have numerical dissipation in a scheme such that the spectral radius is less than unity for increasing values of $\omega\Delta t$. The box method has no numerical dissipation. Finally, Hughes (1977) cites a problem with averaging schemes in general as applied to nonlinear problems. For the nonlinear single degree-of-freedom case, Eq. (4) can be written as

$$\dot{y}^{i}+\dot{y}^{i-1}+\omega^{i}y^{i}+\omega^{i-1}y^{i-1}=0 \qquad (14)$$

The update equation for y^{i}, Eq. (12), becomes

$$y^{i}=\left(\frac{2-\omega^{i-1}\Delta t}{2+\omega^{i}\Delta t}\right)y^{i-1} \qquad (15)$$

and the stability becomes conditional as parameter ω changes with time. The practice suggested by Hughes (1977) for avoiding this problem is to use an averaged value of ω, i.e.,

$$\dot{y}^{i}+\dot{y}^{i-1}+\left(\frac{\omega^{i}+\omega^{i-1}}{2}\right)(y^{i}+y^{i-1})=0 \qquad (16)$$

Generalized-α Method

Given the stability problems associated with the box method, Gobat and Grosenbaugh (2001) proposed replacing the temporal integration with Chung and Hulbert's (1993) generalized-α

Table 1. Algorithms Included in Generalized-α Method

Algorithm	γ	α_k	α_m	1st order problem	2nd order problem
Box method	$\frac{1}{2}$	$\frac{1}{2}$	$\frac{1}{2}$	Ablow and Schechter (1983)	
Backward differences	1	0	0	Koh et al. (1999)	
Generalized trapezoidal	$[\frac{1}{2},1]$	0	0	Sun et al. (1994)	Newmark (1959)
Cornwell and Malkus	$\frac{1}{2}-\alpha$	α	0	Cornwell and Malkus (1992)	Hilber et al. (1977)
WBZ-α	$\frac{1}{2}+\alpha$	0	α		Wood et al. (1981)

method. The generalized-α method is a reasonably complete family of algorithms that is second-order accurate, has controllable numerical dissipation, and offers a clear approach to coefficient averaging for the nonlinear problem. Following Chung and Hulbert's development of the generalized-α method for second-order equations, semidiscrete Eq. (2) becomes

$$(1-\alpha_m)\widetilde{\mathbf{M}}\dot{\mathbf{Y}}^i+\alpha_m\widetilde{\mathbf{M}}\dot{\mathbf{Y}}^{i-1}+(1-\alpha_k)\widetilde{\mathbf{K}}\mathbf{Y}^i+\alpha_k\widetilde{\mathbf{K}}\mathbf{Y}^{i-1}$$

$$+(1-\alpha_k)\widetilde{\mathbf{F}}^i+\alpha_k\widetilde{\mathbf{F}}^{i-1}=0 \qquad (17)$$

The difference equation is the same as for the generalized trapezoidal rule (Hughes 1987),

$$\mathbf{Y}^i=\mathbf{Y}^{i-1}+\Delta t[(1-\gamma)\dot{\mathbf{Y}}^{i-1}+\gamma\dot{\mathbf{Y}}^i] \qquad (18)$$

The three parameter family of algorithms given by Eqs. (17) and (18) defines the generalized-α method for the first-order semidiscrete problem. The method is second-order accurate if

$$\alpha_m-\alpha_k+\gamma=\frac{1}{2} \qquad (19)$$

From the eigenvalues of the amplification matrix, the stability requirement is

$$\alpha_k\leq\frac{1}{2} \quad \alpha_m\leq\frac{1}{2} \quad \gamma\geq\frac{1}{2} \qquad (20)$$

Requiring second-order accuracy according to Eq. (19) and forcing the eigenvalues of the amplification matrix to be equal as $\omega\Delta t\rightarrow\infty$ to prevent bifurcation, yields formulas for α_k and α_m as a function of λ^∞ only

$$\alpha_k=\frac{\lambda^\infty}{\lambda^\infty-1} \quad \alpha_m=\frac{3\lambda^\infty+1}{2\lambda^\infty-2} \qquad (21)$$

This yields a second-order accurate algorithm in which the only parameter is the eigenvalue (or spectral radius) at infinity.

Algorithms that can be obtained through various choices of α_k, α_m, γ, and λ^∞ are listed in Table 1. Spectral radii of some of these algorithms are shown in Fig. 1. Note that taking $\lambda^\infty \in[0,1)$ as the basis for the spectral radius results in a different set of algorithms than $\lambda^\infty \in[-1,0]$. For $\rho^\infty=1$ the only option is the negative eigenvalue and this results in the box method. A nondissipative algorithm with $\lambda^\infty=+1$ cannot be achieved.

In applying the generalized-α method to the nonlinear problem we must choose the time point at which we will evaluate $\widetilde{\mathbf{M}}$, $\widetilde{\mathbf{K}}$, and $\widetilde{\mathbf{F}}$. A natural choice, consistent with the practice suggested by Hughes (1977) for nonlinear first-order problems and exemplified by Eq. (16), is provided by the temporal averaging of terms that is already a part of the method. At time step i Eq. (17) becomes
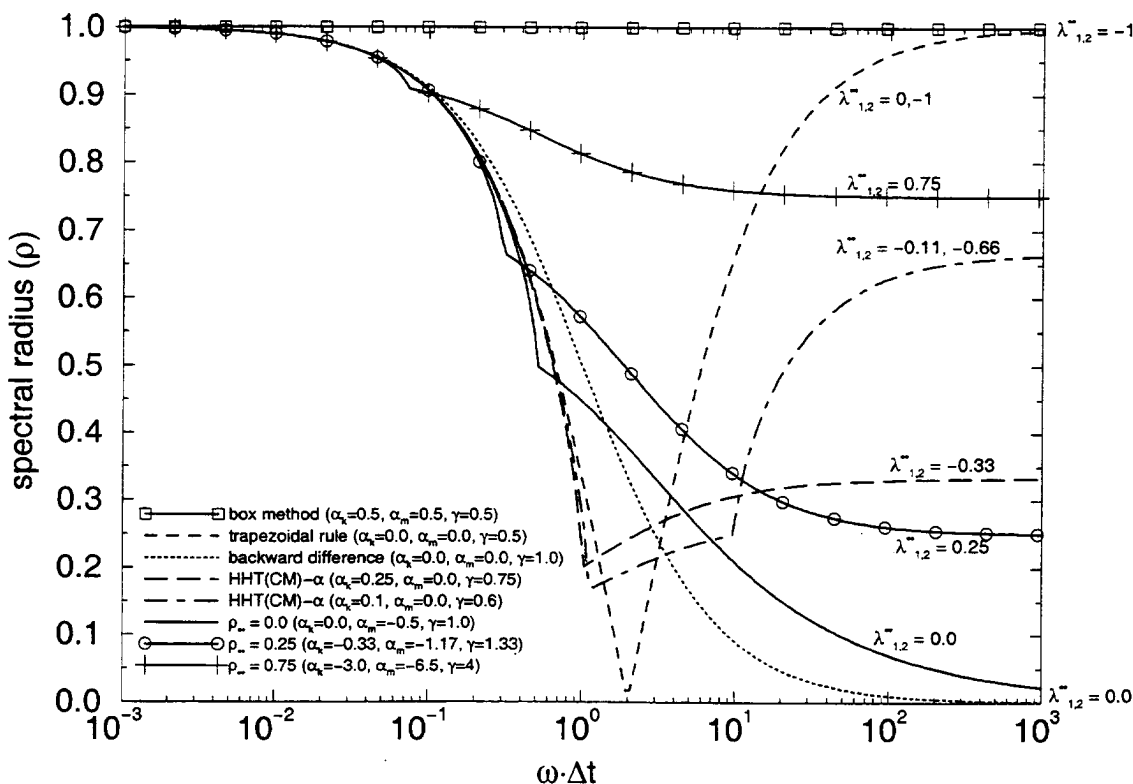

Fig. 1. Spectral radii of generalized-α family algorithms

$$(1-\alpha_m)\widetilde{\mathbf{M}}^{i-\alpha_m}\dot{\mathbf{Y}}^i+\alpha_m\widetilde{\mathbf{M}}^{i-\alpha_m}\dot{\mathbf{Y}}^{i-1}+(1-\alpha_k)\widetilde{\mathbf{K}}^{i-\alpha_k}\mathbf{Y}^i$$

$$+\alpha_k\widetilde{\mathbf{K}}^{i-\alpha_k}\mathbf{Y}^{i-1}+(1-\alpha_k)\widetilde{\mathbf{F}}^i+\alpha_k\widetilde{\mathbf{F}}^{i-1}=0 \qquad (22)$$

where the averaged coefficient matrices are defined as

$$\widetilde{\mathbf{M}}^{i-\alpha_m}=(1-\alpha_m)\widetilde{\mathbf{M}}^i+\alpha_m\widetilde{\mathbf{M}}^{i-1} \qquad (23)$$

$$\widetilde{\mathbf{K}}^{i-\alpha_k}=(1-\alpha_k)\widetilde{\mathbf{K}}^i+\alpha_k\widetilde{\mathbf{K}}^{i-1} \qquad (24)$$

This scheme has been implemented in a computer program for two- and three-dimensional simulations of cable dynamics (Gobat and Grosenbaugh 2000). At each time step, Eq. (22) is solved using a Newton–Raphson procedure. The solution from the previous time step (or the static solution at the initial time step) serves as the initial guess in the nonlinear iterations. Because of this, the ultimate success of the solution is dependent on both the stability of the time integration and on the ability of the nonlinear solver to converge on a solution at time step i given an initial guess based on the solution at time step $i-1$. To improve convergence the program implements an adaptive time stepping scheme whereby the time step (the distance between the guess at $i-1$ and the solution at i) is reduced by factors of 10 at any spots where the solver is not successful. A practical limit of four orders of magnitude below the base-line time step is set to prevent the solution from proceeding in the face of a physical or numerical instability unrelated to the nonlinear solution procedure (e.g., Crank–Nicholson noise).

All of the numerical solutions that follow were obtained using this program. Thus, the box method, trapezoidal rule, and backward difference results, while spectrally equivalent to previous implementations, may be more stable than previous solutions because of the coefficient averaging scheme in Eq. (22). For clarity, spectrally equivalent historical names are retained in discussions of comparative algorithm performance that follow.

Application to Hanging Chain Problem

The performance of the different algorithms that can be implemented with the generalized-α family is studied by considering the free and forced response of the hanging chain shown in Fig. 2. In the free-response problem, we apply a small initial displacement to the chain and then at time $t=0$, release it. The dynamic response of the chain for $t>0$ can be calculated analytically for the small motions that result. In the forced response problem we impose a sinusoidally varying horizontal displacement to the top of the chain and analyze the forced response. This latter problem was studied both numerically and experimentally by Howell and Triantafyllou (1993).

Free Response to Initial Displacement

For small motions and an inextensible chain, the equation of motion is

$$m\frac{\partial^2 q}{\partial t^2}=\frac{\partial}{\partial s}\left[mgs\frac{\partial q}{\partial s}\right] \qquad (25)$$

where $m=$ mass per length of the chain, $q=$ transverse displacement of the chain, $g=$ acceleration due to gravity, and $s=$ independent coordinate along the chain with $s=0$ at the free end. Assuming a harmonic solution of the form

$$q(s,t)=q(s)[A\cos\omega t+B\sin\omega t] \qquad (26)$$
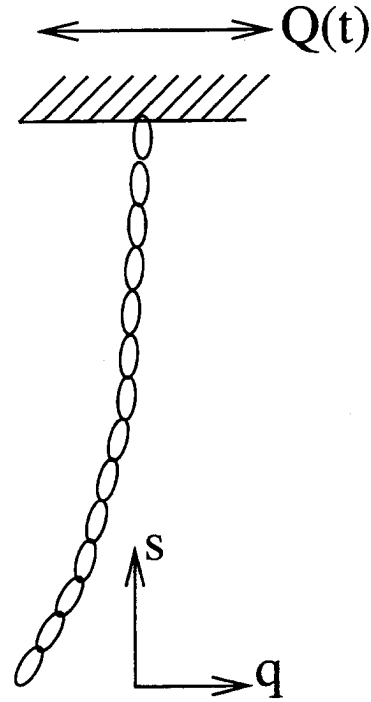
the mode shapes; $q(s)$, are (Triantafyllou et al. 1986)

Fig. 2. Definitions for hanging chains problems

$$q(s)=c_1 J_0\left(2\omega\sqrt{\frac{s}{g}}\right)+c_2 Y_0\left(2\omega\sqrt{\frac{s}{g}}\right) \qquad (27)$$

where J_0 and $Y_0=$ zero-order Bessel functions of the first and second kind, respectively. The requirement that the solution be finite at $s=0$ leads to the elimination of the Y_0 term and the requirement that $q(L)=0$ leads to the natural frequencies, ω. They are given by the roots of

$$J_0\left(2\omega\sqrt{\frac{L}{g}}\right)=0 \qquad (28)$$

The complete response is given as the sum of the response in all modes:

$$q(s,t)=\sum_{n=1}^{\infty}J_0\left(2\omega_n\sqrt{\frac{s}{g}}\right)[A_n\cos\omega t+B_n\sin\omega t] \qquad (29)$$

The coefficients A_n and B_n are determined from the initial displacement, $q_0(s)$, and velocity, $\dot{q}_0(s)$. Given $\dot{q}_0(s)=0$, we can immediately determine that $B_n=0$. To determine A_n we first write

$$q(s,0)=\sum_{n=1}^{\infty}A_n J_0\left(2\omega_n\sqrt{\frac{s}{g}}\right)=q_0(s) \qquad (30)$$

Multiplying both sides by $J_0(2\omega_n\sqrt{s/g})$, integrating from $s=0$ to $s=L$, and making use of the fact that

$$\int_0^L J_0\left(2\omega_n\sqrt{\frac{s}{g}}\right)J_0\left(2\omega_m\sqrt{\frac{s}{g}}\right)ds=0 \quad \text{for } n\neq m \qquad (31)$$

yields the following equation for A_n:

$$A_n=\frac{\int_0^L q_0(s)J_0\left(2\omega_n\sqrt{\frac{s}{g}}\right)ds}{\int_0^L J_0^2\left(2\omega_n\sqrt{\frac{s}{g}}\right)ds} \qquad (32)$$

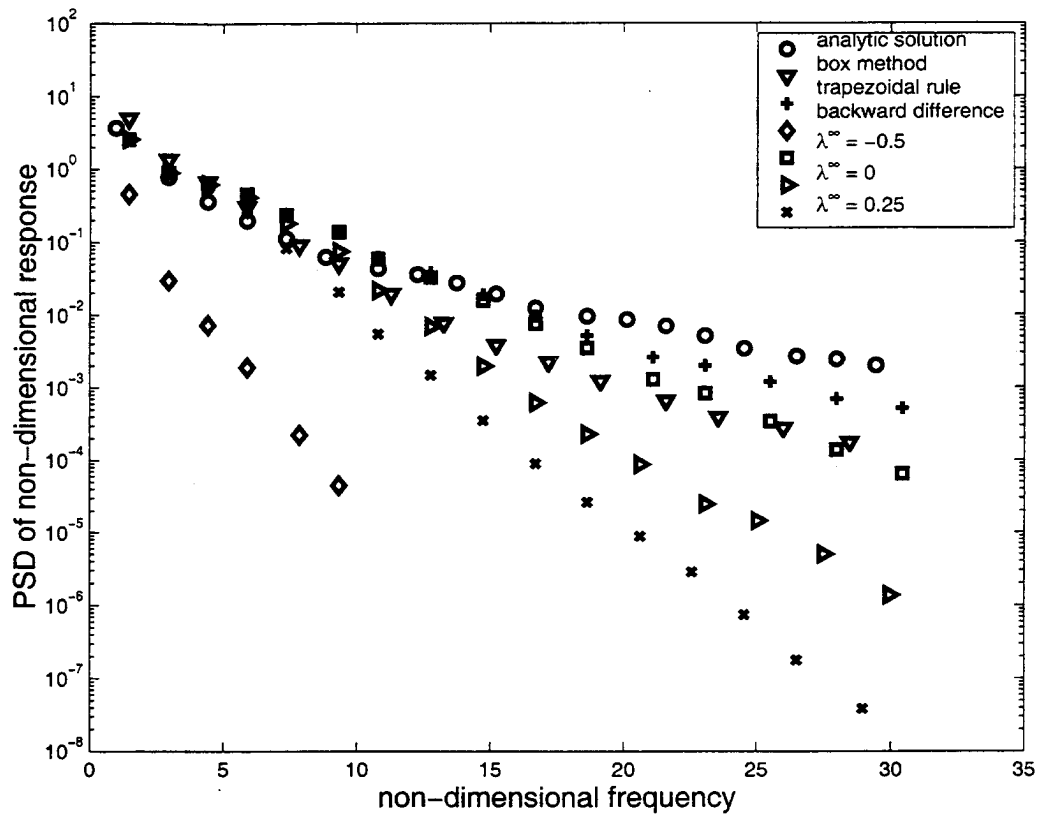**Fig. 3.** Power spectra peaks of response of free end of chain for analytic solution and for six variants of generalized-α method with Δt = 0.01 s and $n = 50$
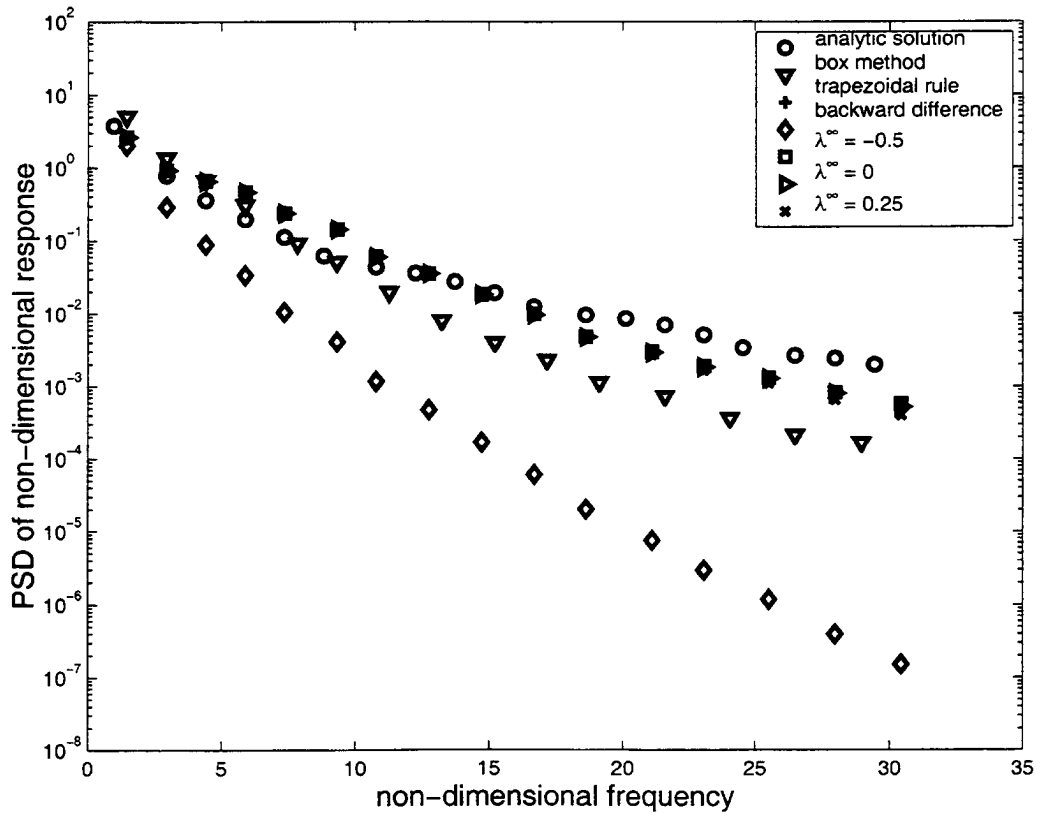

Fig. 4. Power spectra peaks of response of free end of chain for analytic solution and for six variants of generalized-α method with Δt = 0.001 s and $n = 50$
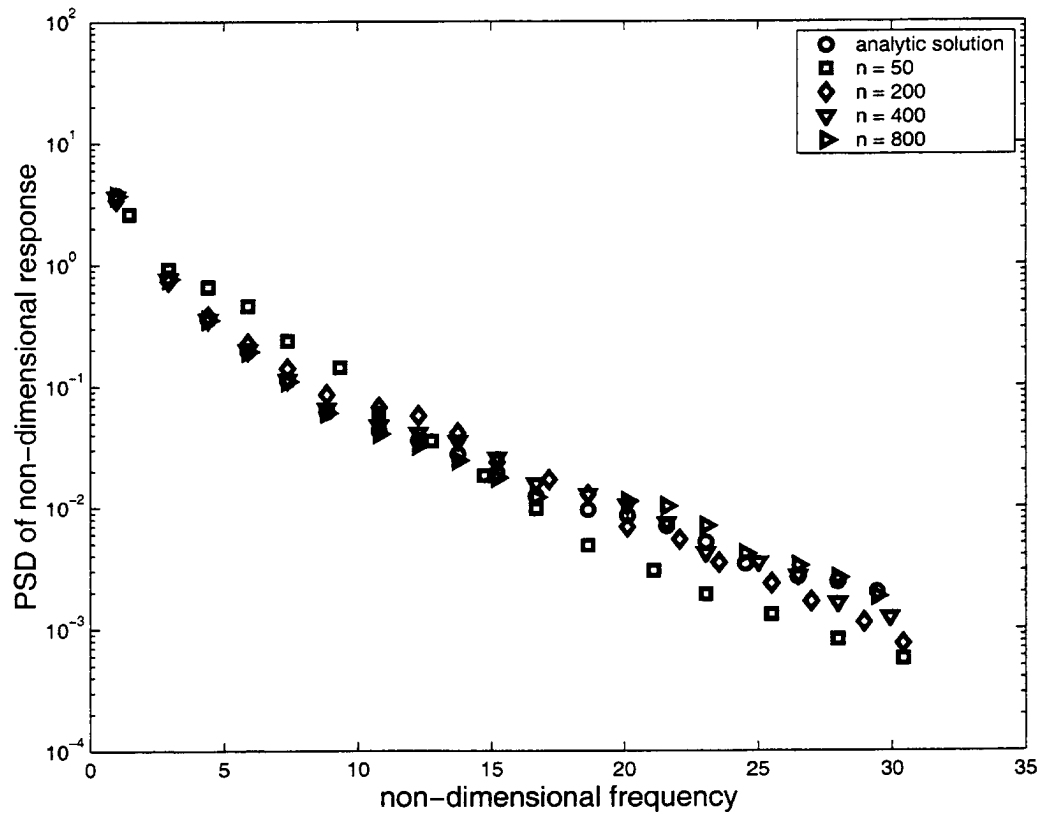
Fig. 5. Power spectra peaks of response of free end of chain for analytic solution and for $\lambda^\infty = -\frac{1}{2}$, $\Delta t = 0.001$ s, with $n = 50, 200, 400,$ and 800
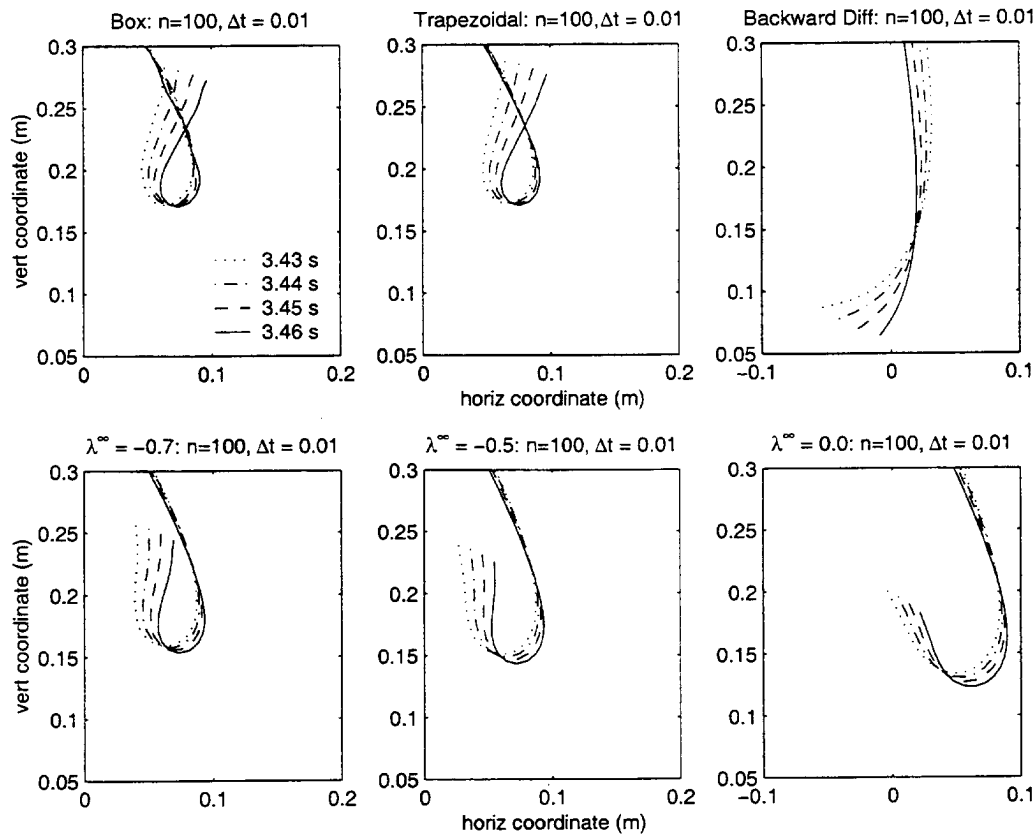

Fig. 6. Snapshots of chain configuration near time of expected intersection for six algorithms that can be obtained from within generalized-α method
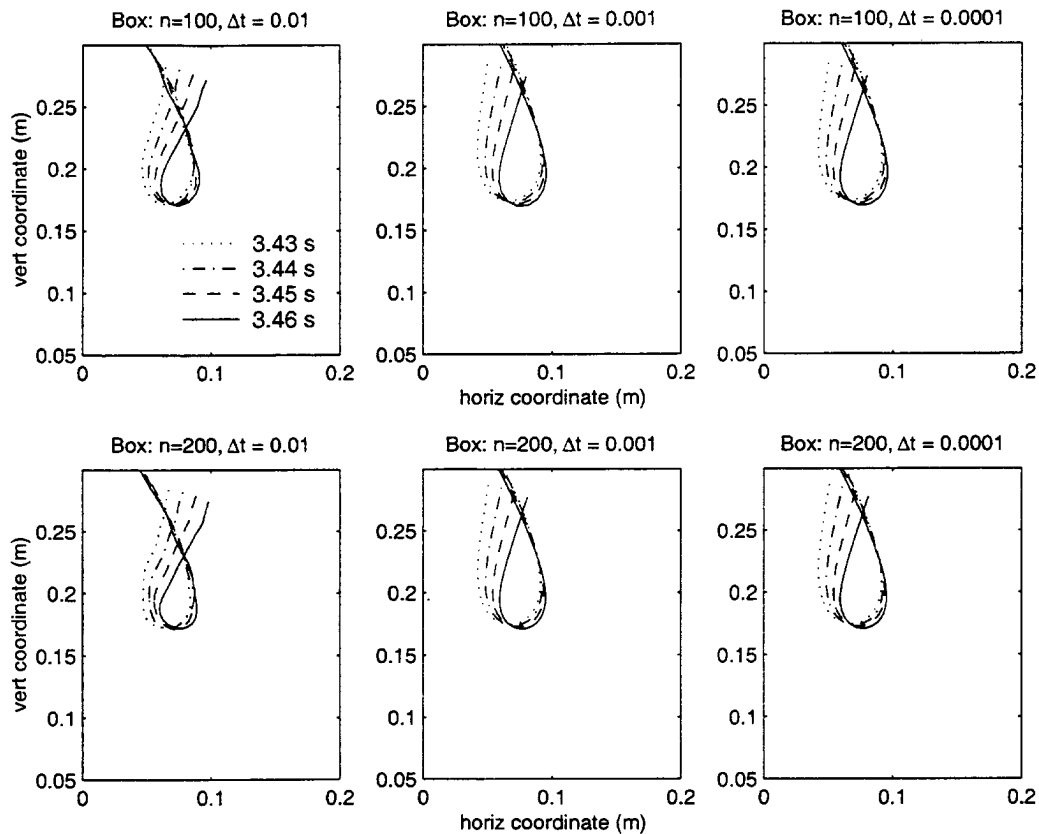
Fig. 7. Snapshots of chain configuration near time of expected intersection for box method with different spatial and temporal discretizations

The analytic solution was computed for a chain released from an initial catenary configuration. For simplicity all of the model parameters (mass per length, gravity, length) were set to unity. The horizontal force applied at $s=0$ to create the initial deflection was set to 0.001 N. All of the integrals for the analytic solution were computed using the trapezoidal rule with 10,000 panels. A 400 s time series of the response at the free end was constructed using the first 20 modes of the analytic solution. The analytic result was sampled at 20 Hz to adequately capture the response up to mode 20. (The natural frequency for mode 20 is approxi-

mately 5 Hz.)

Analytic solutions were compared to numerical simulation results for a chain released from the same initial configuration. For simulation results EI was set to 10^{-6} Nm^2 and EA to 10^9 N. This setting for EI corresponds to the value of $EI^* = EI/mgL^3$ used in Howell's (1992) comparison of experimental and simulation results and in the simulations of the forced hanging chain problem that follow. The results from Howell demonstrated that this value is sufficient to stabilize the numerical solution in the presence of zero tension, but is small enough as to have a negligible effect on
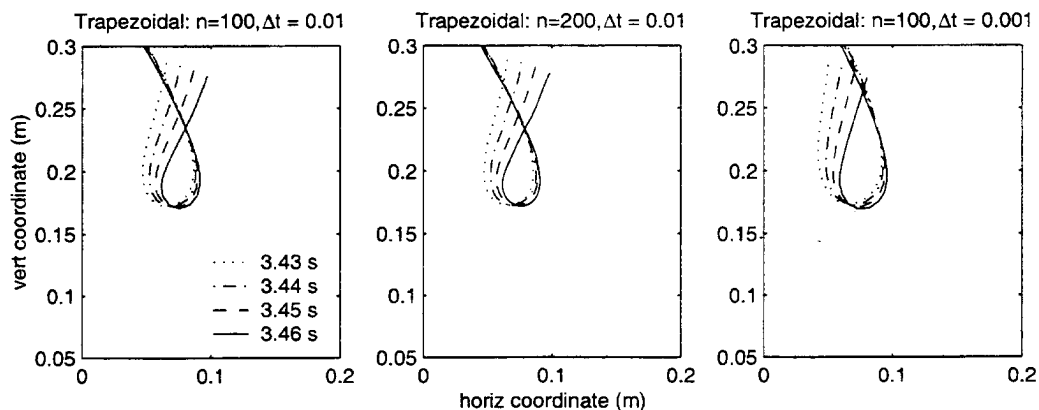

Fig. 8. Snapshots of chain configuration near time of expected intersection for trapezoidal rule with different spatial and temporal discretizations

the accuracy of the simulation result (based on comparisons with experiment). The model results were insensitive to changes in this value of at least an order of magnitude.

Because the primary distinction among the various algorithms contained within the generalized-α family is the amount of numerical dissipation, all results are compared in the frequency domain. For each 400 s time series, power spectra of the response at the free end were computed using nonoverlapping 256 point fast Fourier transforms. For clarity, only the peaks of the spectra are plotted. This prevents clutter and allows for a comparison of the spectral roll off of each of the algorithms compared to the roll off from the analytic solution.

Fig. 3 shows a comparison between the analytic solution and numerical solutions for six different parametrizations of the generalized-α method. At this time step, $\Delta t = 0.01$ s, most of the algorithms are accurate out to the fifth or sixth mode. The notable exception is the first-order accurate backward difference solution, which substantially underestimates the response even in the first mode. All of the algorithms show a marked fall off from the analytic solution at higher frequencies, with the solutions for $\lambda^\infty \geq 0$ showing the most decay and the trapezoidal rule appearing to be the most accurate.

In Fig. 1, the numerical damping of most algorithms increases with increasing $\omega \Delta t$. The idea that we should see less numerical damping at a fixed frequency with a decrease in Δt is illustrated in Fig. 4, which shows the same results comparison as in Fig. 3 for a time step of $\Delta t = 0.001$ s. At this time step most algorithms are accurate out to the tenth mode. Only backward differences, which due to its first-order accuracy is again a poor solution even at very low frequencies, and $\lambda^\infty = 0$ are worse than this.

That the other algorithms, with their varying levels of dissipation, have converged to the same solution suggests that the remaining error is not due to numerical dissipation. Fig. 5 shows the comparison for four cases with $\lambda^\infty = -\frac{1}{2}$ and $\Delta t = 0.001$ s, with a varying number of nodes. As the node density is increased, the numerical model is better able to resolve the mode shapes associated with the higher frequencies. At $n = 800$, the numerical solution is in agreement with the analytic solution over the full range of the analytically computed response.

These results demonstrate that the ability of the model to accurately resolve high-frequency response is dependent on temporal and spatial discretizations and on the numerical dissipation for a given algorithm. Given sufficient temporal and spatial resolution, most of the algorithms appear ultimately capable of accurately calculating the free response of the swinging chain. Based on its better accuracy at the larger time step, the best choice of algorithm for this problem appears to be the trapezoidal rule.

Two-Dimensional Forced Response to Imposed Motion

The forced hanging chain problem that we consider was studied by Howell and Triantafyllou (1993). In this problem, a 1.75-m-long chain is suspended from an actuator which imposes a sinusoidally varying horizontal linear displacement, $Q(t)$, to the top of the chain (Fig. 2). In experiments, Howell and Triantafyllou observed that the free end of the chain intersects the chain above it at approximately 3.4 s.

Fig. 6 shows the configuration of the lower portion of the chain from 3.43 to 3.46 s for six different numerical algorithms, all with $n = 100$ and $\Delta t = 0.01$ s. The box method and trapezoidal rule both closely match the experimental result, with intersection occurring by the 3.43 s mark. For the other algorithms the inter-

section occurs later; the delay in the time of intersection is proportional to the amount of numerical dissipation in the algorithm. The backward differences solution is again the worst; the chain never intersects itself. Likewise for $\lambda^\infty = 0$, though it comes closer to doing so. For $\lambda^\infty = -0.7$, intersection actually happens at 3.47 s and for $\lambda^\infty = -0.5$, at 3.50 s.

The situation changes somewhat if we consider the effect of temporal and spatial discretization. Fig. 7 shows the same time points for versions of the box method with $n = 100$ or 200 and $\Delta t = 0.01$, 0.001, and 0.0001 s. In this case we see that increasing the number of nodes does not significantly affect the solution, suggesting that $n = 100$ is adequate to accurately capture the response. An increase in temporal resolution, however, from $\Delta t = 0.01$ s to $\Delta t = 0.001$ s, leads to a delay in the crossover to approximately 3.46 s. The result at the even smaller $\Delta t = 0.0001$ s confirms that the solution has converged at these smaller time steps. Fig. 8 shows this same behavior for the trapezoidal rule. The only notable difference between trapezoidal rule and box method solutions is the better smoothness of the trapezoidal rule solutions at $\Delta t = 0.01$ s.

Similar results for $\lambda^\infty = -0.5$ are shown in Fig. 9. In this case, the solution at $\Delta t = 0.001$ s is slightly different than the solutions from the trapezoidal rule and the box method at the 3.46 s point. The solutions for $\Delta t = 0.0001$ s are in good agreement with the converged solutions for $\Delta t = 0.001$ s in Figs. 7 and 8. A notable difference in the solutions for the various algorithms does appear between 3.5 and 4.0 s (i.e., following crossover). Both trapezoidal rule and box method solutions required significant adaptation of the time step to get through the collapse of the lower portion of the chain following the crossover. The enhanced stability of solutions with $\lambda^\infty = -0.5$ allowed for a smooth numerical solution in this region, with no or very little adaptation. Without experimental verification, however, we cannot say if the $\lambda^\infty = -0.5$ solution is accurate.

At sufficiently small time steps and adequate spatial resolution, all three algorithms: box method, trapezoidal rule, and $\lambda^\infty = -0.5$, provide accurate solutions. Trapezoidal rule is the best choice in terms of the computational cost of accuracy, where cost is measured in terms of time step. As indicated, however, in regions where the solution becomes numerically unstable some numerical dissipation may be necessary to obtain a solution. This suggests a trade off between optimizing the time step for accuracy and optimizing the algorithm for stability.

Three-Dimensional Forced Response to Imposed Motion

In order to further explore these trade offs, three-dimensional simulations were conducted to explore the behavior of the solutions beyond the time when the chain crosses over itself. Howell (1992) noted that out-of-plane motions of the experimental chain only become significant after this point. The simulations were conducted with a small initial out-of-plane force applied at the free end to promote the initiation of out-of-plane motion. This models the inevitable presence of small disturbing forces that produce instabilities in the two-dimensional motion and eventually lead to a fully three-dimensional (3D) response.

Table 2 lists the observed time of the chain crossing over itself and the total running time (out of a possible 10 s simulation) of the simulation before failure. Only solutions for $-0.4 \leq \lambda^\infty \leq -0.2$ ran for the full 10 s and resulted in an accurate crossover prediction. At $\Delta t = 0.01$ s, the numerically stable solutions (at $\lambda^\infty = -0.3$ and $\lambda^\infty = -0.2$) were less accurate than the two-
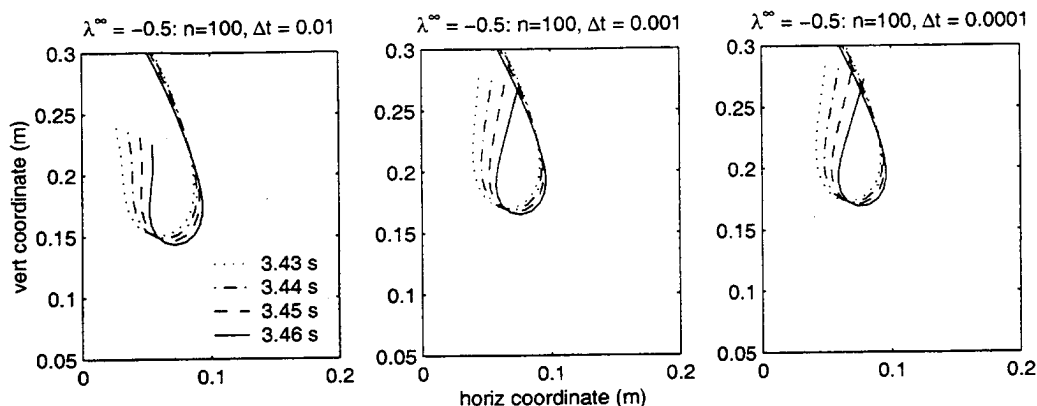
Fig. 9. Snapshots of chain configuration near time of expected intersection for $\lambda^{\infty} = -\frac{1}{2}$ with different spatial and temporal discretizations

Table 2. Crossover Time and Total Runtime in Three-Dimensional Simulations

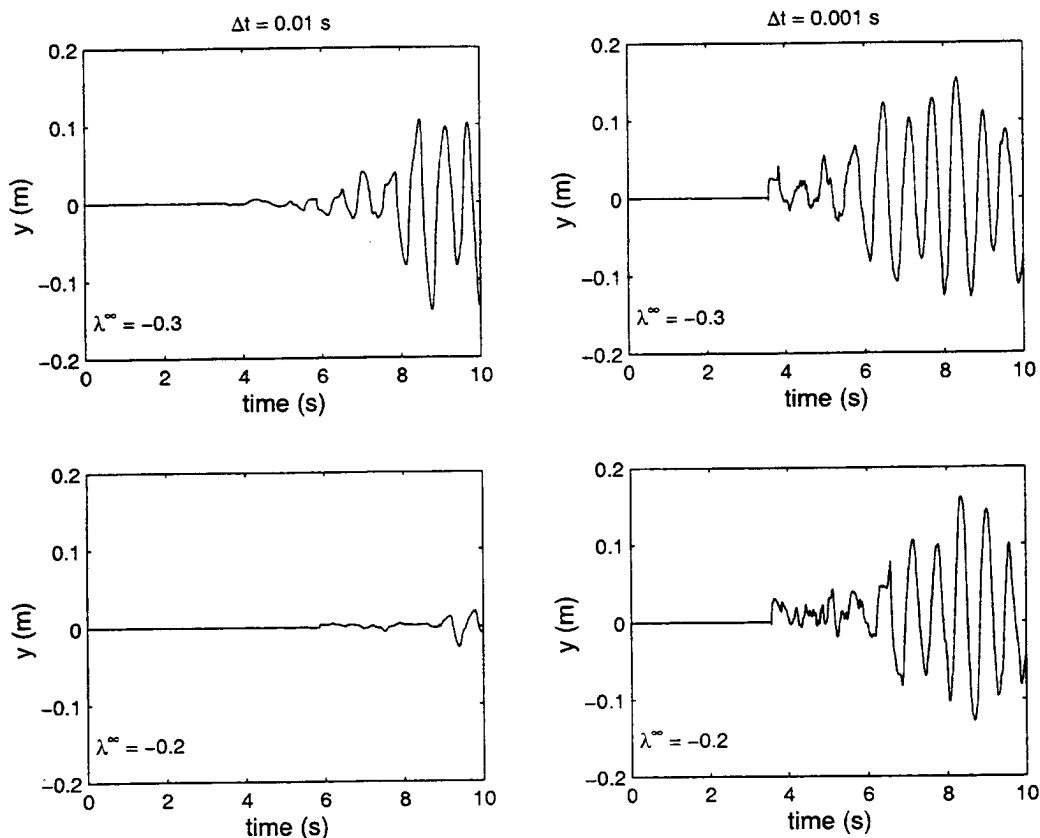| Method	$\Delta t = 0.01$ s		$\Delta t = 0.001$ s	
	Crossover (s)	Run Length (s)	Crossover (s)	Run Length (s)
Box	$\cdots$	3.38	3.45	3.64
Trapezoidal	3.41	3.78	3.45	3.60
$\lambda^{\infty} = -0.7$	$\cdots$	3.40	$\cdots$	3.40
$\lambda^{\infty} = -0.5$	$\cdots$	3.42	$\cdots$	3.40
$\lambda^{\infty} = -0.4$	3.49	3.56	3.46	10.0
$\lambda^{\infty} = -0.3$	3.51	10.0	3.46	10.0
$\lambda^{\infty} = -0.2$	3.52	10.0	3.47	10.0
$\lambda^{\infty} = -0.1$	$\cdots$	3.60	$\cdots$	3.40
$\lambda^{\infty} = 0.0$	$\cdots$	10.0	$\cdots$	3.42
$\lambda^{\infty} = 0.1$	$\cdots$	10.0	$\cdots$	3.42

Fig. 10. Out-of-plane motion of free end of hanging chain for $\lambda^{\infty} = -0.3$ and $\lambda^{\infty} = -0.2$ and $\Delta t = 0.01$ s and $\Delta t = 0.001$ s
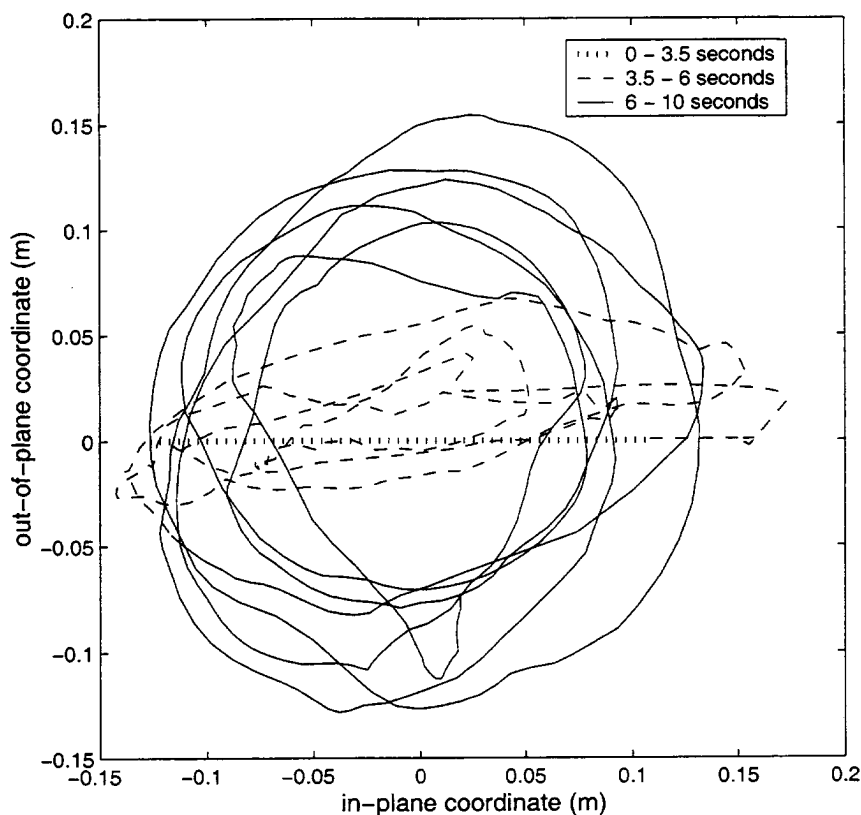
Fig. 11. Trace of horizontal motions of free end of hanging chain for $\lambda^\infty = -0.3$ and $\Delta t = 0.001$ s

dimensional simulations for $\lambda^\infty = -0.5$ at this same time step. This is consistent with the observation that as damping increases the crossover time is delayed. Also consistent with the two-dimensional results is the convergence to a prediction of 3.46 s with an increase in temporal resolution to $\Delta t = 0.001$ s.

The numerical stability of results for $\lambda^\infty = 0.0$ and $\lambda^\infty = 0.1$ at $\Delta t = 0.01$ s, but not at $\Delta t = 0.001$ s, illustrates the dependence of the stability on the frequency content of the response, the time step, and the damping properties of the algorithm. Because the spectral radii in Fig. 1 all initially decrease with the product $\omega \Delta t$, a decrease in Δt at a fixed frequency will result in less damping. If the response at that frequency was responsible for the instability then the solution at the smaller time step may actually be less stable.

Fig. 10 shows the out-of-plane motion of the free end of the chain for the algorithms that ran for the full 10 s at both $\Delta t = 0.01$ s and $\Delta t = 0.001$ s. At $\Delta t = 0.01$ s there is little consistency between the levels of out-of-plane motion predicted by the different algorithms. For the solutions at $\Delta t = 0.001$ s the results for out-of-plane response appear roughly equivalent. A trace of the motion of the free end in the horizontal plane for $\Delta t = 0.001$ s and $\lambda^\infty = -0.3$ is shown in Fig. 11. The roughly circular whirling motion revealed by the trace after the three-dimensional motion is fully developed as expected for this problem (Nayfeh and Mook 1995).

Conclusions

The stability properties of the box, backward difference, trapezoidal rule, and generalized-α temporal integration algorithms were studied. The box method is popular in cable dynamics applica-

tions because it is second-order accurate and easy to implement. In the harmonically driven hanging chain problem considered above, however, its poor numerical stability made solutions difficult or impossible to obtain beyond a certain point in time.

Backward differences have excellent numerical dissipation (and thus very good stability), but are only first-order accurate. For the hanging chain problem this poor accuracy leads to numerical solutions that compared poorly with both analytic and experimental results. Unlike in the experiment, the simulated chain never crossed over itself. Trapezoidal rule solutions showed good accuracy, but because of their weak numerical dissipation, relatively poor stability in the forced response problem. Of the three algorithms that have been popularly employed in cable dynamics problems (box, backward differences, trapezoidal rule) the trapezoidal rule appears to be the best choice.

Of all the algorithms considered, the generalized-α algorithm had the best combination of accuracy and stability. For the harmonically driven chain it was the only algorithm that produced a simulation of the three-dimensional whirling motion that develops after crossover occurs. While it is slightly more complicated to program, it has the advantage that once it is implemented, box, backward difference, and trapezoidal rule solutions can easily be obtained through proper choice of the parameter values. The best choice for λ^∞ is problem dependent, but $-0.5 \le \lambda^\infty \le -0.2$ appears to be a useful range for many problems. Care must still be taken to insure adequate spatial and temporal discretizations so that the important frequency content of the solution is preserved.

Acknowledgment

References

Ablow, C. M., and Schechter, S. (1983). "Numerical simulation of undersea cable dynamics." *Ocean Eng.*, 10, 443–457.

Burgess, J. J. (1993). "Bending stiffness in a simulation of undersea cable deployment." *Int. J. Offshore Polar Eng.*, 3, 197–204.

Chatjigeorgiou, I. K., and Mavrakos, S. A. (1999). "Comparison of numerical methods for predicting the dynamic behavior of mooring lines." *Proc., 9th Int. Offshore and Polar Engineering Conf.*, Brest, France.

Chiou, R. B., and Leonard, J. W. (1991). "Nonlinear hydrodynamic response of curved singly connected cables." *Computer modeling in ocean engineering*, Balkena, Rotterdam, 407–415.

Chung, J., and Hulbert, G. (1993). "A time integration algorithm for structural dynamics with improved numerical dissipation." *J. Appl. Mech.*, 60, 371–375.

Chung, J., and Hulbert, G. M. (1994). "A family of single-step Houbolt time integration algorithms for structural dynamics." *Comput. Methods Appl. Mech. Eng.*, 118, 1–11.

Cornwell, R. E., and Malkus, D. S. (1992). "Improved numerical dissipation for time integration algorithms in conduction heat transfer." *Comput. Methods Appl. Mech. Eng.*, 97, 149–156.

Gobat, J. I., and Grosenbaugh, M. A. (2000). "WHOI Cable v2.0: Time domain numerical simulation of moored and towed oceanographic systems." *Tech. Rep. No. WHOI-2000-08*, Woods Hole Oceanographic Institution.

Gobat, J. I., and Grosenbaugh, M. A. (2001). "Application of the generalized-α method to the time integration of the cable dynamics equations." *Comput. Methods Appl. Mech. Eng.*, 190, 4817–4829.

Hilber, H. M., Hughes, T. J. R., and Taylor, R. L. (1977). "Improved numerical dissipation for time integration algorithms in structural dynamics." *Earthquake Eng. Struct. Dyn.*, 5, 283–292.

Howell, C. T. (1992). "Investigation of the dynamics of low-tension cables." PhD thesis, Massachusetts Institute of Technology and Woods Hole Oceanographic Institution Joint Program, Woods Hole, Mass.

Howell, C. T., and Triantfyllou, M. S. (1993). "Stable and unstable nonlinear resonant response of hanging chains: theory and experiment." *Proc. R. Soc. London, Ser. A*, 440, 345–364.

Hughes, T. J. R. (1977). "Unconditionally stable algorithms for nonlinear heat conduction." *Comput. Methods Appl. Mech. Eng.*, 10, 135–139.

Hughes, T. J. R. (1987). *The finite element method: Linear static and dynamic finite element analysis*, Prentice-Hall, Englewood Cliffs, NJ.

Koh, C. G., Zhang, Y., and Quek, S. T. (1999). "Low-tension cable dynamics: Numerical and experimental studies." *J. Eng. Mech.*, 125(3), 347–354.

Nayfeh, A. H., and Mook, D. T. (1995). *Nonlinear oscillations*, Wiley Classic Library, ed., Wiley-Interscience, New York.

Newmark, N. M. (1959). "A method of computation for structural dynamics." *J. Eng. Mech.*, 85(3), 67–94.

Sun, Y., Leonard, J. W., and Chiou, R. B. (1994). "Simulation of unsteady oceanic cable deployment by direct integration with suppression." *Ocean Eng.*, 21, 243–256.

Thomas, D. O. (1993). "A numerical investigation of time integration schemes applied to the dynamic solution of mooring lines." PhD thesis, Univ. Newcastle upon Tyne, Newcastle, U.K.

Triantafyllou, M. S., and Howell, C. T. (1993). "Nonlinear unstable response of hanging chains." *J. Sound Vib.*, 162, 263–280.

Triantafyllou, M. S., Bliek, A., Burgess, J., and Shin, H. (1986). "Mooring dynamic for offshore applications: Part 1 theory." *Tech. Rep. No. MITSG 86-1*, MIT Sea Grant College Program.

Wood, W. L., Bossak, M., and Zienkiewicz, O. C. (1981). "An alpha modification of Newmark's method." *Int. J. Numer. Methods Eng.*, 15, 1562–1566.